Hindawi
Mathematical Problems in Engineering
Volume 2018, Article ID 7090186, 9 pages
https://doi.org/10.1155/2018/7090186

Research Article

Efficient 3D Volume Reconstruction from a Point Cloud Using a Phase-Field Method

Darae Jeong,[1] **Yibao Li**,[2] **Heon Ju Lee**,[3] **Sang Min Lee**,[3] **Junxiang Yang**,[1] **Seungwoo Park**,[1] **Hyundong Kim**,[1] **Yongho Choi**,[1] **and Junseok Kim**[1]

[1]*Department of Mathematics, Korea University, Seoul 02841, Republic of Korea*
[2]*School of Mathematics and Statistics, Xi'an Jiaotong University, Xi'an 710049, China*
[3]*ROKIT Inc., Seoul 08512, Republic of Korea*

Correspondence should be addressed to Junseok Kim; cfdkim@korea.ac.kr

Received 22 November 2017; Accepted 1 January 2018; Published 6 February 2018

Academic Editor: Costică Moroșanu

We propose an explicit hybrid numerical method for the efficient 3D volume reconstruction from unorganized point clouds using a phase-field method. The proposed three-dimensional volume reconstruction algorithm is based on the 3D binary image segmentation method. First, we define a narrow band domain embedding the unorganized point cloud and an edge indicating function. Second, we define a good initial phase-field function which speeds up the computation significantly. Third, we use a recently developed explicit hybrid numerical method for solving the three-dimensional image segmentation model to obtain efficient volume reconstruction from point cloud data. In order to demonstrate the practical applicability of the proposed method, we perform various numerical experiments.

1. Introduction

In this paper, we propose an efficient and robust algorithm for volume reconstruction from a point cloud. Reconstructing the three-dimensional model from a point cloud is important in medical applications. Surface reconstruction from a point cloud is a process of finding a surface model that approximates an unknown surface for a given set of sample points lying on or near the unknown surface [1].

Hoppe et al. developed an algorithm to reconstruct a surface in the three-dimensional space from unorganized points scattered on or near the unknown surface. The algorithm is based on the idea of determining the zero level set of a signed distance function [2]. Kazhdan proposed a surface reconstruction method which takes an oriented point set and returns a solid model. The method uses Stokes' theorem to calculate the characteristic function (one inside the model and zero outside of it) of the solid model [3]. To reconstruct implicit surfaces from scattered unorganized data set, Li et al. presented a novel numerical method for surface embedding narrow volume reconstruction from unorganized points [4, 5]. Yang et al. proposed a 3D reconstruction technique from nonuniform point clouds via local hierarchical clustering [6]. Zhao et al. developed a fast sweeping level set and tagging methods [7]. Yezzi Jr. et al. proposed a new medical image segmentation based on feature-based metrics on a given image [8].

Beneš et al. used the Allen-Cahn equation with a forcing term to achieve image segmentation [9]. Caselles et al. proposed a model for active contours which could extract smooth shapes and could be adapted to find several contours simultaneously [10]. Methods using geometric active contour were introduced in [11–14]. Zhang et al. developed a weighted sparse penalty and a weighted grouping effect penalty in modeling the subspace structure [15]. Chen used an ICKFCM method (ICA analysis and KFCM algorithm) in medical image segmentation and made a good result in extracting the complicated images [16]. Zhang et al. proposed a novel fuzzy level set method based on finding the minimum of energy function to locate the true object boundaries effectively [17]. Other numerical studies based on level set method were also introduced in [18, 19].

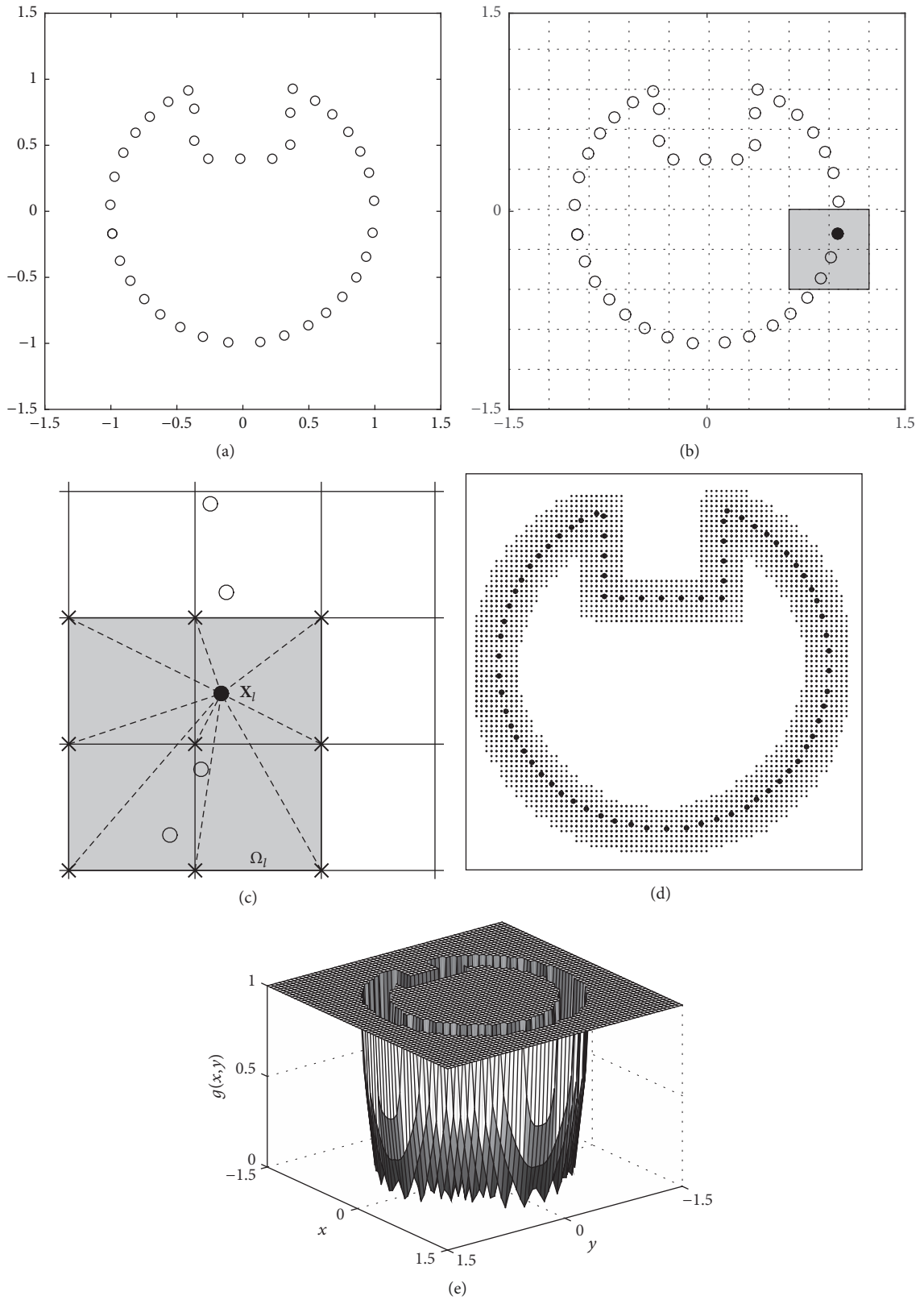

Figure 1: Schematic of defined distance function. (a) Point cloud data, (b) mesh grid covering the point cloud and local mesh grid, (c) local mesh grid Ω_l embedding a point $\mathbf{X}_l$, (d) narrow band domain, and (e) edge indicator function, $g(\mathbf{x})$.

In this article, we propose an explicit hybrid algorithm for volume reconstruction from a point cloud. Therefore, it does not need implicit solvers such as multigrid methods. The computation is fast and efficient because the proposed algorithm uses a narrow band domain and a good initial condition.

This paper is organized as follows. In Section 2, we describe a mathematical model and a numerical solution algorithm for volume reconstruction from a point cloud. We present the numerical results for several examples in Section 3. In Section 4, we conclude.

2. Mathematical Model and Numerical Solution Algorithm

Now, we propose an explicit hybrid numerical method for volume reconstruction from a point cloud using a phase-field method. For $\mathbf{X}_l = (X_l, Y_l)$ in the two-dimensional space or $\mathbf{X}_l = (X_l, Y_l, Z_l)$ in the three-dimensional space, $S = \{\mathbf{X}_l \mid 1 \le l \le N\}$ denote the point cloud in the two- or the three-dimensional space, respectively. The geometric active contour model based on the mean curvature motion is given by the following evolution equation [20]:

$$\frac{\partial \phi(\mathbf{x},t)}{\partial t} = g(\mathbf{x})\left[-\frac{F'(\phi(\mathbf{x},t))}{\epsilon^2} + \Delta\phi(\mathbf{x},t) + \lambda F(\phi(\mathbf{x},t))\right], \tag{1}$$

where $g(\mathbf{x})$ is an edge indicator function, $F(\phi) = 0.25(\phi^2 - 1)^2$, and ϵ is a constant which is related to the phase transition width. Note that here we use a different edge indicator function and efficient explicit numerical algorithm.

For simplicity of exposition, we first discretize (1) in the two-dimensional space $\Omega = (a,b) \times (c,d)$. Let $h = (b-a)/(N_x - 1) = (d-c)/(N_y - 1)$ be the uniform mesh size, where N_x and N_y are the number of grid points. Let $\Omega_h = \{\mathbf{x} = (x_i, y_j) : x_i = a + (i-1)h,\ y_j = c + (j-1)h,\ 1 \le i \le N_x,\ 1 \le j \le N_y\}$ be the discrete domain. Let ϕ_{ij}^n be approximations of $\phi(x_i, y_j, n\Delta t)$, where Δt is the time step. Let $d(\mathbf{x}) = \mathrm{dist}(\mathbf{x}, S) = \min_{1\le l\le N}|\mathbf{X}_l - \mathbf{x}|$ be the distance to the data S, where $\mathbf{X}_l = (X_l, Y_l)$. In fact, we will use the distance function as an edge indicator function, $g(\mathbf{x})$. In practice, for $l = 1, \ldots, N$, we define a local domain Ω_l which embeds the point $\mathbf{X}_l$ and set the minimum value at the grid point between the point and the grid point. For example, Ω_l is a 3×3 grid. Then, the computational narrow band domain is defined as

$$\Omega_{\mathrm{nb}} = \bigcup_{l=1}^{N} \Omega_l. \tag{2}$$

Outside the narrow band domain, we set a large value to the edge indicator function, see Figure 1 for the procedure.

In this study, we apply the simplest sequential splitting procedure. We split (1) into two equations by using the operator splitting method:

$$\frac{\partial \phi(\mathbf{x},t)}{\partial t} = g(\mathbf{x})\left[\Delta\phi(\mathbf{x},t) + \lambda F(\phi(\mathbf{x},t))\right], \tag{3}$$

$$\frac{\partial \phi(\mathbf{x},t)}{\partial t} = -g(\mathbf{x})\frac{F'(\phi(\mathbf{x},t))}{\epsilon^2} = g(\mathbf{x})\frac{\phi(\mathbf{x},t) - \phi^3(\mathbf{x},t)}{\epsilon^2}. \tag{4}$$

For a good initial configuration, we set $\phi_{ij}^0 = 1$ inside on the narrow band domain and set $\phi_{ij}^0 = -1$ outside the narrow band domain.

Given ϕ^n, we solve (3) on the narrow band domain Ω_{nb} by using the explicit Euler method:

$$\frac{\phi_{ij}^* - \phi_{ij}^n}{\Delta t} = g_{ij}\left[\Delta_d \phi_{ij}^n + \lambda F\left(\phi_{ij}^n\right)\right], \tag{5}$$

where ϕ_{ij}^* is the intermediate value which is defined at point (x_i, y_j). The initial values at inside and outside region of the narrow band domain Ω_{nb} act as Dirichlet boundary condition in computing the discrete Laplace operator, Δ_d.

Then, we analytically solve (4) by the method of separation of variables [21, 22]. That is, $\phi_{ij}^{n+1} = \psi(\Delta t)$ by analytically solving

$$\frac{d\psi(t)}{dt} = g_{ij}\frac{\psi(t) - \psi^3(t)}{\epsilon^2} \quad \text{with the initial condition } \psi(0) = \phi_{ij}^*. \tag{6}$$

The analytic solution is given as

$$\phi_{ij}^{n+1} = \frac{\phi_{ij}^*}{\sqrt{e^{-2g_{ij}\Delta t/\epsilon^2} + \left(\phi_{ij}^*\right)^2\left(1 - e^{-2g_{ij}\Delta t/\epsilon^2}\right)}}. \tag{7}$$

Therefore, (5) and (7) consist of an efficient and robust algorithm for volume reconstruction from a point cloud. We should note that the proposed numerical solution algorithm is fully explicit. Therefore, we do not need an iterative method such as multigrid method to solve the governing equation. Also, the implementation of the algorithm is straightforward.

3. Computational Experiments

3.1. Two-Dimensional Experiments

3.1.1. Motion by Mean Curvature. To test the proposed numerical scheme, we perform a numerical experiment. The test is motion by mean curvature. If we set $g(\mathbf{x}) = 1$ and $\lambda = 0$, then the governing equation (1) becomes the original Allen-Cahn equation [23], which is a reaction-diffusion equation describing the process of phase separation in a binary alloy

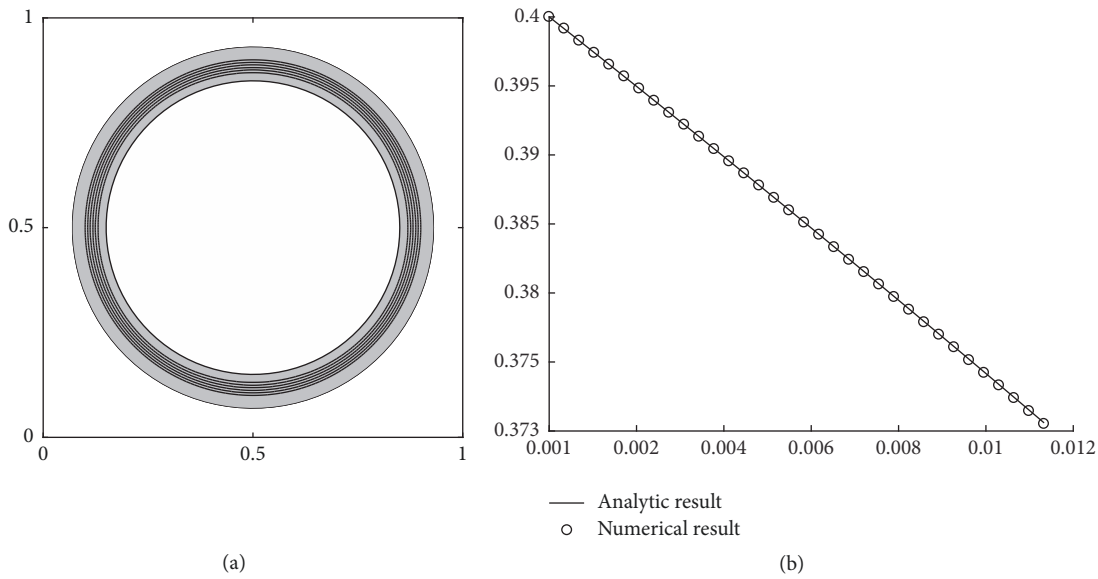

FIGURE 2: Temporal evolutions of the radius with $\Delta t = 0.15h^2$ up to $t = 5000\Delta t$ in the two-dimensional space. (a) Zero level contour and (b) radius $R(t)$ of circle with respect to time.

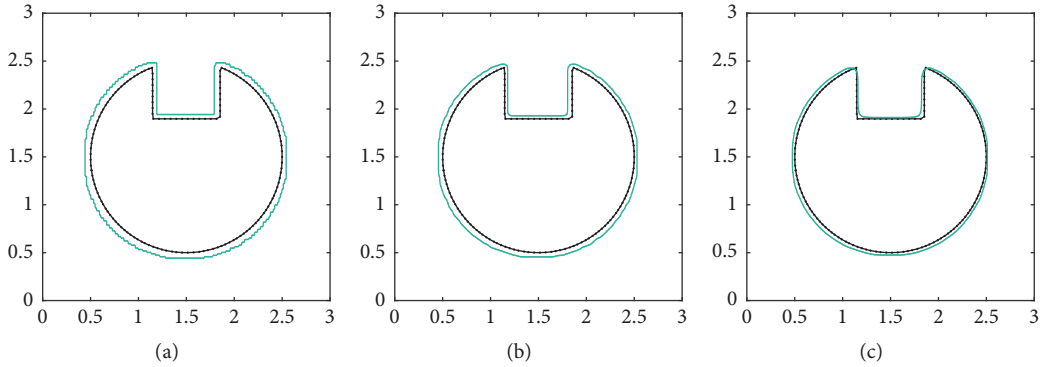

FIGURE 3: Temporal evolution of the interface: (a) initial condition, (b) 100 iterations, and (c) 1000 iterations.

mixture. In the two-dimensional case, as ϵ approaches zero, the zero level set of ϕ evolves with the following velocity:

$$V = -\kappa = -\frac{1}{R}, \tag{8}$$

where V is the normal velocity, κ is the curvature, and R is the radius of curvature at the point of the zero level set [24]. Then, (8) is rewritten by $dR(t)/dt = -1/R(t)$ with $R(0) = R_0$. Therefore, analytic solution is given as $R(t) = \sqrt{R_0^2 - 2t}$.

On the computational domain $\Omega = (0,1) \times (0,1)$, we investigate the motion by mean curvature of the circle in the annulus narrow band domain: $\{(x,y) \mid 0.35 \leq \sqrt{(x-0.5)^2 + (y-0.5)^2} \leq 0.43\}$ as shown in Figure 2(a). We define an initial condition as

$$\phi(x,y,0) = \tanh \frac{R_0 - \sqrt{(x-0.5)^2 + (y-0.5)^2}}{\sqrt{2}\epsilon}. \tag{9}$$

In this numerical simulation, we use the following parameters: $R_0 = 0.4$, $\epsilon = 0.011$, $h = 1/256$, $\Delta t = 0.15h^2$, and $T = 5000\Delta t$. Figures 2(a) and 2(b) show the temporal evolution of the initial circle and its radius with respect to time, respectively. For verification of our numerical results, we include the results of the analytic solution. As shown in Figure 2, the initial circle shrinks under the motion by mean curvature.

3.1.2. The Basic Working Mechanism of the Algorithm. The edge indicator function $g(\mathbf{x})$ is close to zero where the point cloud exists. Therefore, the evolution will stop or slow down in the neighborhood of the point cloud. In (1), $\partial\phi/\partial t = -F'(\phi)/\epsilon^2 + \Delta\phi$ makes the phase-field shrink until it reaches the point cloud by the mean curvature flow. If the geometry of the point cloud is not convex, then the term $\lambda F(\phi)$ makes the level set of the phase-field further shrink. For more details, please refer to [20]. To confirm the working mechanism of the algorithm, the temporal evolution of the interface in the two-dimensional space is shown in Figure 3. Here, we use

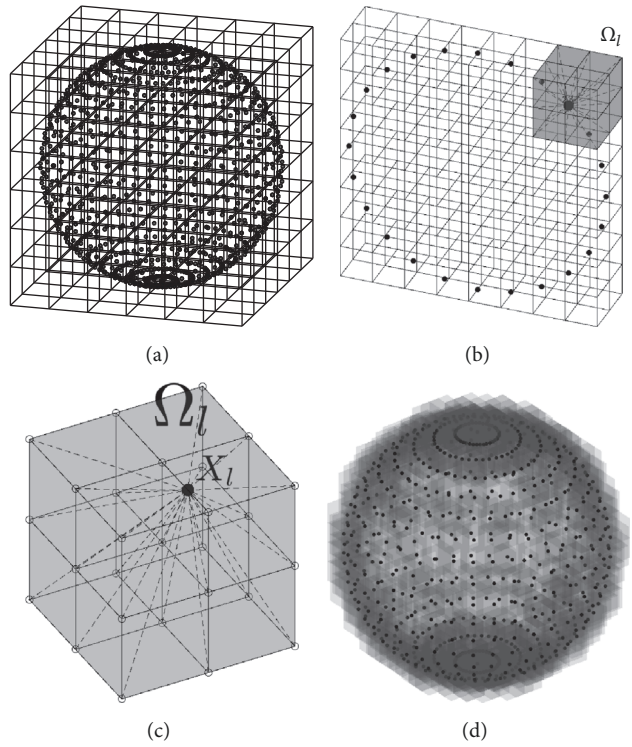

Figure 4: Construction of the three-dimensional distance function $d(\mathbf{x})$ and the narrow band domain: (a) point cloud data and mesh, (b) cross section of point cloud and a local mesh Ω_l of single point $\mathbf{X}_l$, (c) local mesh grid Ω_l embedding a point $\mathbf{X}_l$, and (d) narrow band domain which is determined by the distance function.

the following parameters: $\epsilon = 0.0096$, $h = 1/200$, and $\Delta t = 2.8284e - 5$.

3.2. Three-Dimensional Experiments. Next, we discretize (1) in the three-dimensional space, that is, $\Omega = (a,b) \times (c,d) \times (e,f)$. Let $h = (b-a)/(N_x - 1) = (d-c)/(N_y - 1) = (f-e)/(N_z - 1)$ be the uniform mesh size, where N_x, N_y, and N_z are the total number of grid points. Let $\Omega_h = \{\mathbf{x} = (x_i, y_j, z_k) : x_i = a + (i-1)h,\ y_j = c + (j-1)h,\ z_k = e + (k-1)h,\ 1 \le i \le N_x,\ 1 \le j \le N_y,\ 1 \le k \le N_z\}$ be the discrete domain. We define ϕ_{ijk}^n as approximations of $\phi(x_i, y_j, z_k, n\Delta t)$, where Δt is the time step size. Let $d(\mathbf{x}) = \mathrm{dist}(\mathbf{x}, S) = \min_{1 \le l \le N} |\mathbf{X}_l - \mathbf{x}|$ be the distance to the data S, where $\mathbf{X}_l = (X_l, Y_l, Z_l)$.

Figure 4 represents construction of the three-dimensional distance function $d(\mathbf{x})$ and the narrow band domain. In Figures 4(a) and 4(b), we can see the given point cloud data on computational grid and a local mesh Ω_l of single point $\mathbf{X}_l$. Here, we calculate the distance between the given point $\mathbf{X}_l$ and the grid points $\mathbf{x}$ on the local mesh Ω_l. The distance function $d(\mathbf{x})$ is defined by the shortest one among the distance. Then, we obtain the narrow band domain which is determined by the distance function.

Now, we can straightforwardly extend the two-dimensional numerical solutions (5) and (7) to the following three-dimensional solutions:

$$\frac{\phi_{ijk}^* - \phi_{ijk}^n}{\Delta t} = g_{ijk}\left(\Delta_d \phi_{ijk}^n + \lambda F\left(\phi_{ijk}^n\right)\right),$$

$$\phi_{ijk}^{n+1} = \frac{\phi_{ijk}^*}{\sqrt{e^{-2g_{ijk}\Delta t/\epsilon^2} + \left(\phi_{ijk}^*\right)^2\left(1 - e^{-2g_{ijk}\Delta t/\epsilon^2}\right)}}. \tag{10}$$

3.2.1. Reconstruction from Various Point Clouds. First, we reconstruct volume of Happy Buddha from the given scattered points ($N = 1621848$) as shown in Figure 5(a) [25]. For numerical test, we use the following parameters: $\epsilon = 0.0069$, $h = 0.0048$, $\Delta t = h/(200\sqrt{3})$, $N_x = 250$, $N_y = 500$, $N_z = 250$, $\Omega = (0, 1.2) \times (0, 2.4) \times (0, 1.2)$, and $\lambda = 100$. In the first and second rows in Figure 5, we can see the front and back views of Happy Buddha. By the proposed scheme, we obtain the numerical solution ϕ after 200 iterations (see Figure 5(c)) with the initial condition in Figure 5(b).

Next, we reconstruct volume of Armadillo model from the given scattered points ($N = 129732$) as shown in Figure 6(a) [25]. For numerical test, we use the following parameters: $\epsilon = 0.0127$, $h = 0.0088$, $\Delta t = h/(200\sqrt{3})$, $N_x = 220$, $N_y = 250$, $N_z = 200$, $\Omega = (0, 2.2) \times (0, 2.5) \times (0, 2)$, and $\lambda = 1000$. In the first and second rows in Figure 6, we can see the front and back views of Armadillo model. By the proposed scheme, we obtain the numerical solution ϕ after 400 iterations (see Figure 6(c)) with the initial condition in Figure 6(b).

As the final example, we reconstruct volume of Stanford Dragon from the given scattered points ($N = 656469$) as shown in Figure 7(a) [25]. For numerical test, we use the

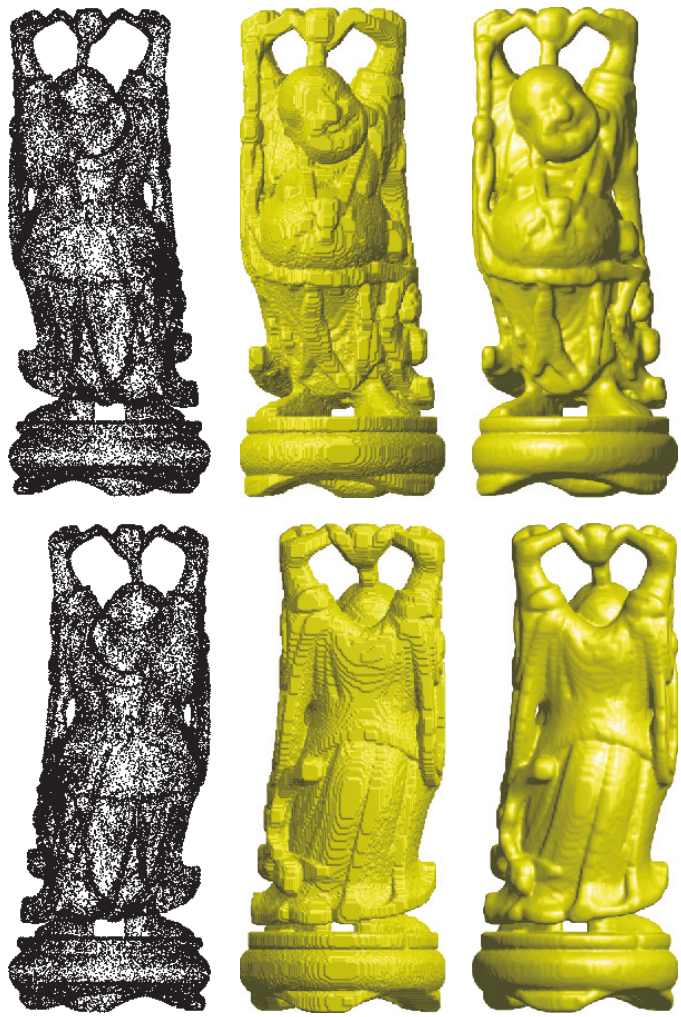

(a) (b) (c)

Figure 5: Front and back views of Happy Buddha: (a) point clouds, (b) initial condition of ϕ, and (c) numerical solution ϕ after 200 iterations.

following parameters: $\epsilon = 0.00432$, $h = 0.003$, $\Delta t = h/(200\sqrt{3})$, $N_x = 400$, $N_y = 320$, $N_z = 240$, $\Omega = (0, 1.2) \times (0, 1) \times (0, 0.8)$, and $\lambda = 100$. In the first and second rows in Figure 7, we can see the front and back views of Stanford Dragon. By the proposed scheme, we obtain the numerical solution ϕ after 400 iterations (see Figure 7(c)) with the initial condition in Figure 7(b).

3.2.2. Effect of λ. In this section, we investigate the effect of λ parameter on the three-dimensional volume reconstruction. The parameter makes the level set of ϕ shrink to the given points. We use the same parameters in Figure 7 except for the λ value. As shown in Figure 8, if the value of λ is small, then the surface is oversmoothed by the motion by mean curvature. On the other hand, if it is too large, then the surface is rough.

4. Conclusions

In this article, we developed an explicit hybrid numerical algorithm for the efficient 3D volume reconstruction from unorganized point clouds using a modified Allen-Cahn equation. The 3D volume reconstruction algorithm is based on the 3D binary image segmentation method. The proposed algorithm has potential to be used in various practical industry such as 3D model printing from scattered scanned data. The computational results confirmed that the algorithm is very efficient and robust in reconstructing 3D volume from point clouds.

Conflicts of Interest

The authors declare that they have no conflicts of interest.

Acknowledgments

The first author (D. Jeong) was supported by the National Research Foundation of Korea (NRF) grant funded by the Korean Government (MSIP) (NRF-2017R1E1A1A03070953). The corresponding author (Junseok Kim) was supported by Basic Science Research Program through the National Research Foundation of Korea (NRF) funded by the Ministry

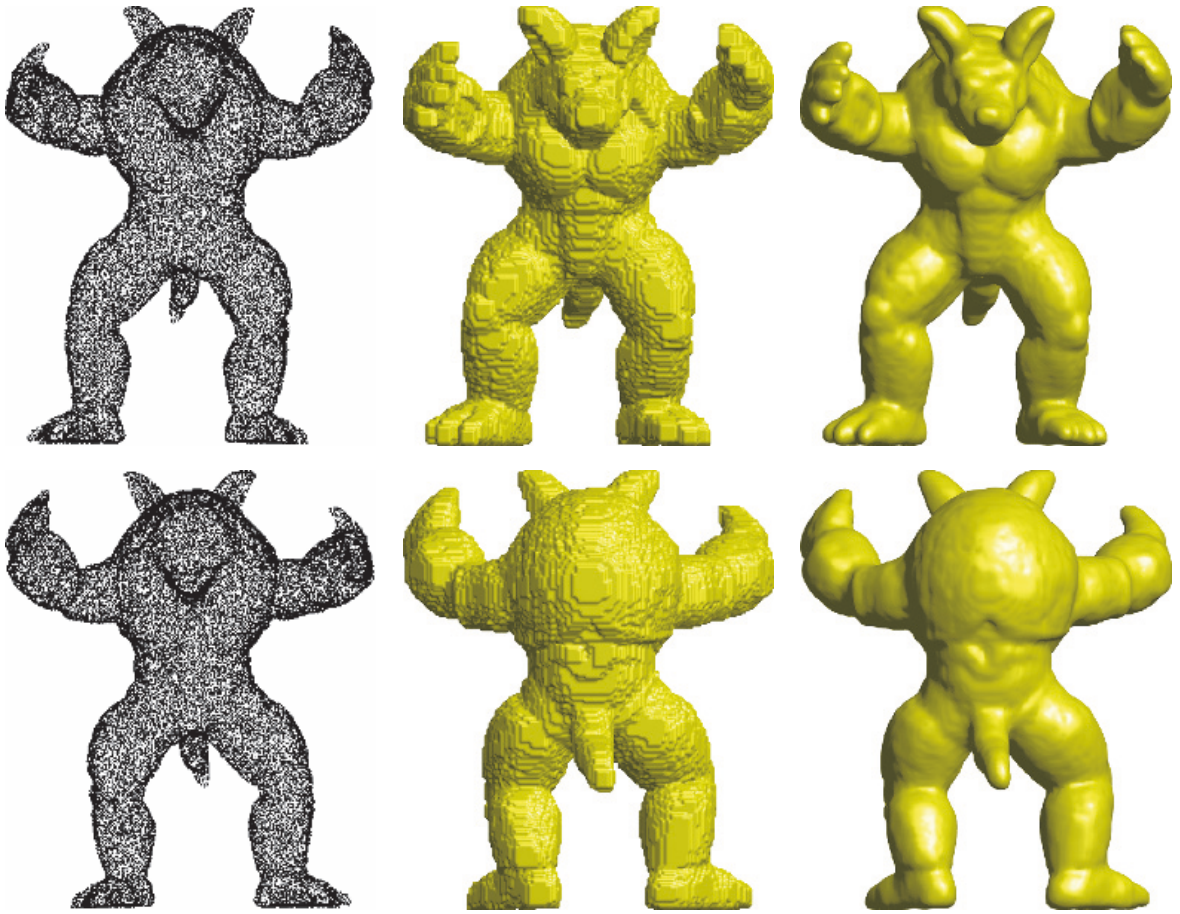

(a) (b) (c)

Figure 6: Front and back views of Armadillo model: (a) initial point clouds, (b) initial condition of ϕ, and (c) numerical solution ϕ after 400 iterations.

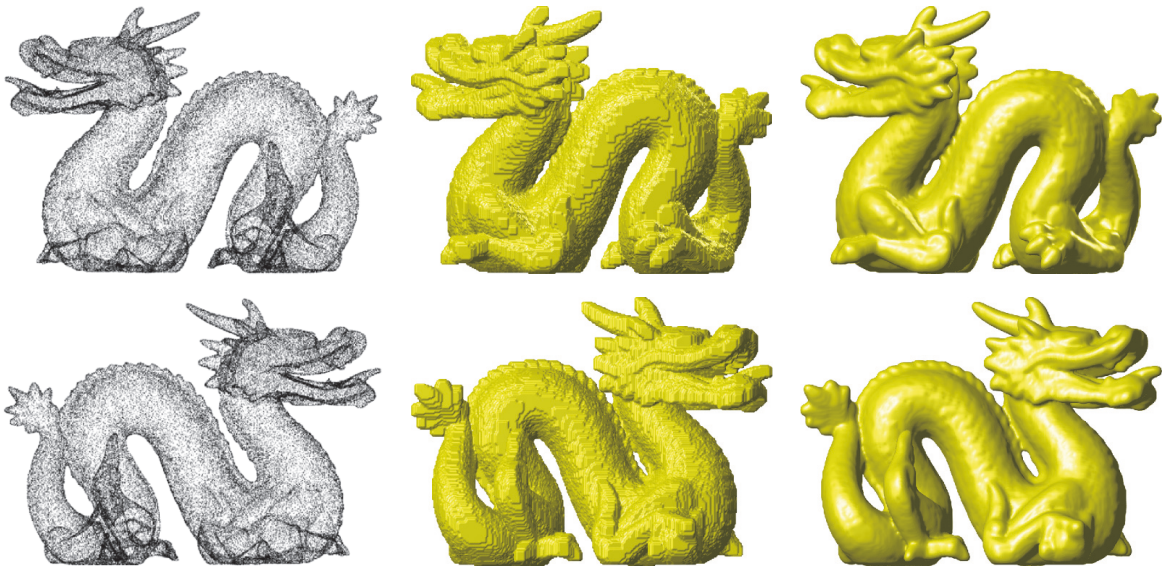

(a) (b) (c)

Figure 7: Front and back views of Stanford Dragon model: (a) initial point clouds, (b) initial condition of ϕ, and (c) numerical solution ϕ after 400 iterations.

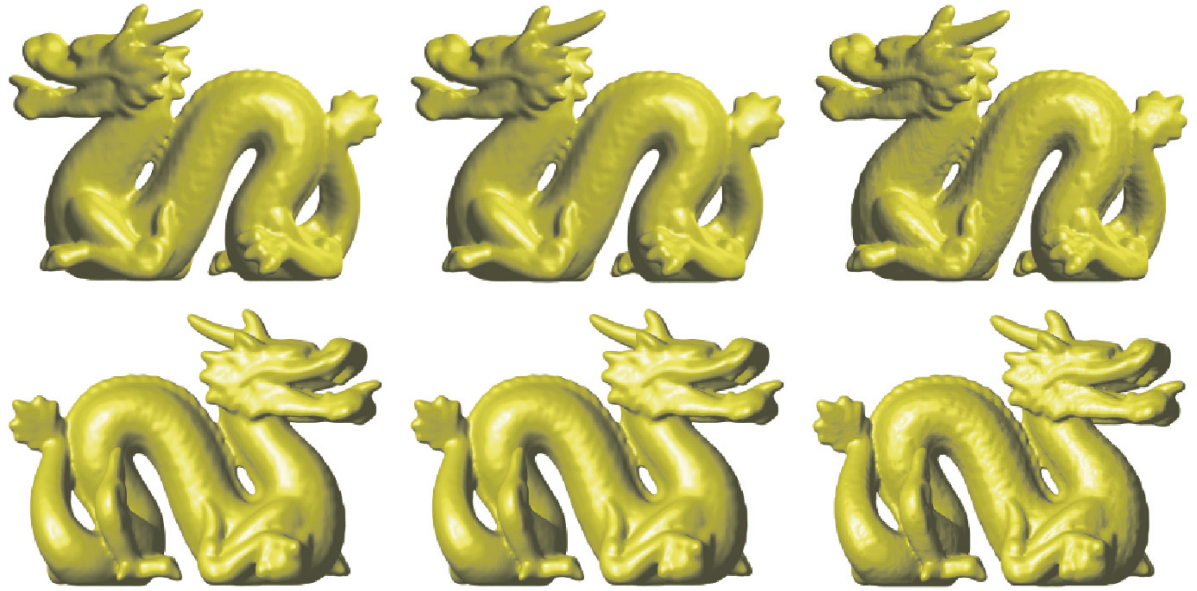

Figure 8: Front and back views of Stanford Dragon model with various λ. Numerical solution ϕ after 1000 iterations.

of Education (NRF-2016R1D1A1B03933243). This work was supported by the BK21 PLUS program.

References

[1] F. Remondino, "From point cloud to surface: the modeling and visualization problem," in *Proceedings of the International Archives of the Photogrammetry, Remote Sensing and Spatial Information Sciences*, vol. XXXIV-5/W10, 2003.

[2] H. Hoppe, T. DeRose, T. Duchamp, J. McDonald, and W. Stuetzle, "Surface reconstruction from unorganized points," *Computer Graphics*, vol. 26, no. 2, pp. 71–78, 1992.

[3] M. Kazhdan, "Reconstruction of solid models from oriented point sets," in *Proceedings of the third Eurographics Symposium on Geometry Processing*, pp. 73–82, 2005.

[4] Y. Li, D. Lee, C. Lee et al., "Surface embedding narrow volume reconstruction from unorganized points," *Computer Vision and Image Understanding*, vol. 121, pp. 100–107, 2014.

[5] Y. Li and J. Kim, "Fast and efficient narrow volume reconstruction from scattered data," *Pattern Recognition*, vol. 48, no. 12, article no. 5459, pp. 4057–4069, 2015.

[6] J. Yang, R. Li, Y. Xiao, and Z. Cao, "3D reconstruction from non-uniform point clouds via local hierarchical clustering," in *Proceedings of the 9th International Conference on Digital Image Processing, ICDIP 2017*, China, May 2017.

[7] H.-K. Zhao, S. Osher, and R. Fedkiw, "Fast surface reconstruction using the level set method," in *Proceedings of the IEEE Workshop on Variational and Level Set Methods in Computer Vision, VLSM 2001*, pp. 194–199, can.

[8] A. Yezzi Jr., S. Kichenassamy, A. Kumar, P. Olver, and A. Tannenbaum, "A geometric snake model for segmentation of medical imagery," *IEEE Transactions on Medical Imaging*, vol. 16, no. 2, pp. 199–209, 1997.

[9] M. Beneš, V. r. Chalupecky, and K. Mikula, "Geometrical image segmentation by the Allen-Cahn equation," *Applied Numerical Mathematics*, vol. 51, no. 2-3, pp. 187–205, 2004.

[10] V. Caselles, F. Catte, T. Coll, and F. Dibos, "A geometric model for active contours in image processing," *Numerische Mathematik*, vol. 66, no. 1, pp. 1–31, 1993.

[11] V. Caselles, R. Kimmel, and G. Sapiro, "Geodesic active contours," *International Journal of Computer Vision*, vol. 22, no. 1, pp. 61–79, 1997.

[12] T. F. Chan and L. A. Vese, "Active contours without edges," *IEEE Transactions on Image Processing*, vol. 10, no. 2, pp. 266–277, 2001.

[13] J. Hahn and C.-O. Lee, "Geometric attraction-driven flow for image segmentation and boundary detection," *Journal of Visual Communication and Image Representation*, vol. 21, no. 1, pp. 56–66, 2010.

[14] S. Kichenassamy, A. Kumar, P. Olver, A. Tannenbaum, and J. Yezzi, "Conformal curvature flows: from phase transitions to active vision," *Archive for Rational Mechanics and Analysis*, vol. 134, no. 3, pp. 275–301, 1996.

[15] B. Zhang, W. Wang, and X. Feng, "Subspace Clustering with Sparsity and Grouping Effect," *Mathematical Problems in Engineering*, vol. 2017, Article ID 4787039, 9 pages, 2017.

[16] Y.-T. Chen, "Medical Image Segmentation Using Independent Component Analysis-Based Kernelized Fuzzy c-Means Clustering," *Mathematical Problems in Engineering*, vol. 2017, Article ID 5892039, 21 pages, 2017.

[17] Y. Zhang, J. Xu, and H. D. Cheng, "A Novel Fuzzy Level Set Approach for Image Contour Detection," *Mathematical Problems in Engineering*, vol. 2016, Article ID 2602647, 12 pages, 2016.

[18] C. Li, C. Xu, C. Gui, and M. D. Fox, "Level set evolution without re-initialization: a new variational formulation," in *Proceedings of the IEEE Computer Society Conference on Computer Vision and Pattern Recognition (CVPR '05)*, pp. 430–436, June 2005.

[19] L. A. Vese and T. F. Chan, "A multiphase level set framework for image segmentation using the Mumford and Shah model," *International Journal of Computer Vision*, vol. 50, no. 3, pp. 271–293, 2002.

[20] Y. Li and J. Kim, "A fast and accurate numerical method for medical image segmentation," *Journal of the Korean Society for Industrial and Applied Mathematics*, vol. 14, no. 4, pp. 201–210, 2010.

[21] A. M. Stuart and A. R. Humphries, *Dynamical Systems and Numerical Analysis*, vol. 2, Cambridge University Press, New York, NY, USA, 1998.

[22] Y. Li, H. G. Lee, D. Jeong, and J. Kim, "An unconditionally stable hybrid numerical method for solving the Allen-Cahn equation," *Computers & Mathematics with Applications. An International Journal*, vol. 60, no. 6, pp. 1591–1606, 2010.

[23] S. M. Allen and J. W. Cahn, "A microscopic theory for antiphase boundary motion and its application to antiphase domain coarsening," *Acta Metallurgica et Materialia*, vol. 27, no. 6, pp. 1085–1095, 1979.

[24] B. Appleton and H. Talbot, "Globally optimal geodesic active contours," *Journal of Mathematical Imaging and Vision*, vol. 23, no. 1, pp. 67–86, 2005.

[25] Stanford university computer graphics laboratory, http://lightfield.stanford.edu/acq.html.